Global and Planetary Change 170 (2018) 34–47

Contents lists available at ScienceDirect

Global and Planetary Change

journal homepage: www.elsevier.com/locate/gloplacha

Research article

The Last Glacial Maximum and Heinrich event I on the Iberian Peninsula: A regional climate modelling study for understanding human settlement patterns

Patrick Ludwig[a,b,*], Yaping Shao[b], Martin Kehl[c], Gerd-Christian Weniger[d]

[a] Institute of Meteorology and Climate Research, Karlsruhe Institute of Technology, Karlsruhe, Germany
[b] Institute for Geophysics and Meteorology, University of Cologne, Cologne, Germany
[c] Institute of Geography, University of Cologne, Cologne, Germany
[d] Neanderthal Museum, Mettmann, Germany

ARTICLE INFO

Keywords:
Last Glacial Maximum
Heinrich event 1
Iberia
Human settlement pattern
Regional climate modelling
Climate change

ABSTRACT

The spatial distribution and dating of archaeological sites suggest a poor occupation of southern Iberia by hunter-gatherers after the Last Glacial Maximum (LGM) and during Heinrich event 1 (H1) compared to Northern Iberia. The H1 was a period of cold and arid climate conditions and is suspected to have played an important role in the population dynamics in Europe at the end of the Pleistocene. In this study, the potential influence of climate change on the human settlement patterns in Iberia is analysed based on regional palaeoclimate modelling. Here, the WRF model is used to simulate continuous time slices of 30 years of climate conditions representative for both the LGM and H1 at high spatial resolution. The model results indicate that, apart from a general decrease in temperature, a considerable decrease in precipitation over southern Iberia occurred during the H1, that agrees with the available climate proxy data. The analysis of ombrotypes unveils extremely arid conditions, particularly over southern Iberia and during the growing season (summer), which could have constrained the availability of food and water to the inhabitants. The total area in Iberia that can be characterized as ultrahyperarid in summer enlarged from 2% (13 K km^2) during the LGM to 22% (148 K km^2) during the H1. Likewise, the reconstruction of vegetation types shows an increase of non-arboreal (open shrubland, grassland) types at the expense of arboreal types in southern Iberia for H1. Thus, the different climate conditions and changes in palaeovegetation between the LGM and H1 probably played a major role in the decrease of the hunter-gatherer populations in southern Iberia.

1. Introduction

Population dynamics in Europe at the end of the Pleistocene (ca. 30–11-ky ago) and its linkage to climate change have been addressed in several recent studies and are subjects of active research (e.g. Banks et al., 2008; Maier et al., 2016; Burke et al., 2017). The time period, characterized by generally cold and dry conditions, encompasses distinctive chronological events including the Last Glacial Maximum (LGM, 23–19 ky ago, Mix et al., 2001) and the Heinrich Event 1 (H1). Heinrich events sensu stricto are defined by enhanced ice-rafted debris in marine deposits of the North Atlantic, the so-called Heinrich layers (Heinrich, 1988). Heinrich events have been associated with the Greenland stadials, in which the layers accumulated, hence defined as Heinrich stadials (Sanchez Goñi and Harrison, 2010). The timing of H1 is estimated as 18–15.6 ky ago (Sanchez Goñi and Harrison, 2010), 18–15 ky ago (Álvarez-Solas et al., 2011) or for the wider H1 sequence at 19–14.6 ky ago (Stanford et al., 2011). In line with the different climate stages, a cultural shift of hunter-gatherer communities from the Solutrean to the Magdalenian techno-complex in Iberia is recognizable (Turrero et al., 2013).

The reconstruction of the LGM climate, both based on proxy data and global climate model (GCM) data, e.g., in the framework of the Paleoclimate Model Intercomparison Project Phase 3 (PMIP3, Braconnot et al., 2012), has received much exposure. Based on pollen data (Bartlein et al., 2011) the mean annual temperatures in Europe was about 11 K colder near the ice sheet and 5 K colder in the Mediterranean realm in comparison to the modern climate and mean annual precipitation was likely to be lower by between 650 mm (northwestern Iberia) and 96 mm (southeastern Iberia). Moreno et al. (2012) presented a climate reconstruction for the last glacial cycle in Iberia based

* Corresponding author at: Karlsruhe Institute of Technology (KIT), Institute of Meteorology and Climate Research, PO Box 3640, 76021 Karlsruhe, Germany.
E-mail address: patrick.ludwig@kit.edu (P. Ludwig).

https://doi.org/10.1016/j.gloplacha.2018.08.006
Received 8 January 2018; Received in revised form 10 August 2018; Accepted 10 August 2018
Available online 13 August 2018
0921-8181/ © 2018 Elsevier B.V. All rights reserved.

on lacustrine sediments. In their study, the LGM was found to be cold and dry, while the following H1 was associated with even lower temperatures and drier hydrological conditions. This change in palaeoclimate conditions is also reflected in many other geological archives in and around Iberia such as the peatbogs of Padul and Navarrés (Pons and Reille, 1988), speleothems of El Pindal cave or Eagle cave (Moreno et al., 2010; Domínguez-Villar et al., 2013) or marine sediments retrieved off the west coast of Portugal or from the Alborán Sea (e.g., Naughton et al., 2016; Fletcher and Sánchez Goñi, 2008; Combourieu Nebout et al., 2009). Overall, the availability of climate proxy data for the time of interest in Iberia is excellent, in particular for its northern part (Moreno et al., 2012, 2014), while less information is available for palaeoclimate changes in the South.

Proxy data are also used for interpretation and qualify the evaluation of GCM palaeo-climate simulations. For most of the existing GCM LGM simulations, the climate in Iberia is too humid when compared to proxy data, particularly along the western coast (e.g. Kageyama et al., 1999; Beghin et al., 2016; Ludwig et al., 2016). Kageyama et al. (1999) and Ludwig et al. (2016) attributed the wet conditions to an enhanced and southward shifted storm track activity over Iberia. Additionally, Ludwig et al. (2016) found that the sea surface temperature (SST) is too warm in some GCMs over parts of the North Atlantic Ocean, which is associated with an enhanced moisture transport towards Europe. Beghin et al. (2016) separated precipitation into summer (when convective precipitation dominated) and winter (when large-scale effects dominated) rainfall and found that the latter accounts much of the overestimation of precipitation. Thus, the understanding of the different mechanisms resulting in too wet conditions might help to understand the range of climate signals from proxy data archives, especially if the proxy data is sensitive to seasonal climate conditions (Beghin et al., 2016) or even to climate extremes (Kageyama et al., 2006). Therefore, the application of regional climate models (RCM) to palaeoclimate conditions is a necessary (Harrison et al., 2015; Beghin et al., 2016) and a promising step forward (Ludwig et al., 2017) to gain a better representation of the climate variability of the past. Although RCMs depend on the large-scale forcing of the GCM data, they allow for a much more detailed resolution of physical processes in the atmosphere, more realistic representation of the topography and resolving feedback mechanisms on the regional scale (Feser et al., 2011; Ludwig et al., 2018). An added value of RCM simulations is most evident for hydrological variables and near-surface winds especially over regions with complex terrain including coastal areas (Ludwig et al., 2018), whereby the former is of particular importance for this study. As shown by Ludwig et al. (2017), the application of an RCM under LGM conditions reveal generally drier climate conditions over Iberia compared to its driving GCM counterpart. Until now, RCMs have been only occasionally used for palaeoclimate studies (e.g. Renssen et al., 2001; Kageyama et al., 2005; Strandberg et al., 2011; Gómez-Navarro et al., 2015; Ludwig et al., 2017).

The long tradition of palaeolithic research in Iberia in combination with a large number of archaeological sites in caves and rock shelters and open-air sites provide a good picture of cultural traditions, defined as techno-complexes and their changes in time. Site distribution and frequency indicate diachronic and regional changes in land use and settlement pattern (Schmidt et al., 2012; Burke et al., 2014; Burke et al., 2017). These changes were probably controlled by climate related changes in palaeoenvironment to which hunter-gatherers had to adapt (Bradtmöller et al., 2012). The role of rapid climate change related to Heinrich events has been stressed in this context. As depicted in Fig. 1, the Solutrean occupation during the LGM is represented by a large number of sites located both in south and north Iberia. In contrast, the Magdalenian occupation, more or less concomitant with H1, shows a decrease of human occupation in southern Iberia compared to the site distribution of the Solutrean.

In this study, the capability of the RCM to simulate the different climate stages at high spatial resolution is considered based on a comparison with available proxy data. Additionally, the link between climate change, palaeovegetation and different settlement patterns during the LGM and H1 is investigated based on the regional palaeoclimate simulation and archaeological observations. An overview of the archaeological data, the configuration of the RCM simulations and the analysis techniques is given in Section 2. In Section 3, the RCM simulations for the present-day conditions are validated, the differences between the LGM and H1 climates are summarized and the results of the derived ombrotypes are described. Furthermore, the results of a logistic regression for potential human existence are presented in the climate change context. Section 4 summarizes and discusses on the new findings.

2. Data and methods

2.1. Archaeological data

We compiled a database of archaeological sites in Iberia including caves, rock shelters and open-air sites. Archaeological layers in these sites were attributed to either the Solutrean or the Magdalenian cultures. The main information about the sites was derived from the literature study and stratigraphically reliable sites were selected by enforcing a strict procedure. Only those with well-documented stratigraphy and clear cultural attribution of the layers were included, while sites without securely attributed layers due to low artefact number or lack of typical typological features were not included. In addition, sites without proper excavation or surface collections lacking stratigraphic context were excluded. Sites with reworked layers were also left out, even if they yielded techno-complexes clearly identified as belonging to Solutrean or Magdalenian. According to accelerator mass spectrometry radiocarbon ages on charcoal or bone, these cultures date to the interval between about 24 ka and 20 ka (Solutrean) and 20.5 to 13 ka BP. This is roughly equal with the interval between the end of H2 (24.3 ka; Sanchez Goñi and Harrison, 2010) and the end of Greenland Interstadial (GI) 1 (~13 ka). The Magdalenian occupation thus took place during H1 and during GI1. Archaeological indicators of the Magdalenian do not suggest a clear discriminability between these two climatic phases, and limited geochronological data is available for making such a distinction. Therefore, we selected all Magdalenian sites which fulfilled the abovementioned criteria. Overall, the selection included 260 sites (Fig. 1b) with lithic industries attributed to the Solutrean (at 144 sites) and/or the Magdalenian (at 176 sites).

2.2. Regional climate modelling

The Weather and Research Forecast model (WRF, Skamarock et al., 2008) is applied to obtain high-resolution palaeoclimate data for the LGM and H1 in Iberia. A preindustrial (PI) simulation is used as a reference for comparison with the LGM and H1 simulations. The WRF model has been successfully configured and tested for simulations of palaeoclimate under glacial conditions (Ludwig et al., 2017). A double nesting is necessary to achieve the desired resolution of 12.5 km. Therefore, the PI and LGM simulations of the Max-Planck-Institute Earth System Model in Palaeoclimate mode (MPI-ESM-P, Stevens et al., 2013) are first downscaled with the WRF model on a 50 km horizontal grid (Ludwig et al., 2017) for the domain shown in Fig. 1a. In the second nesting step, the 50 km data serve as the initial and boundary data for the 30-year continuous PI and LGM simulations on the 12.5 km grid over Iberia (Fig. 1a). To obtain H1 boundary conditions, the MPI-ESM-P LGM sea surface temperatures (SST) are gradually lowered over the North Atlantic (Fig. 1a) with a maximum reduction between 40° and 50°N by 4 K following Kageyama et al. (2005). Additionally, the sea ice cover has been adjusted to the lower SST, so that ocean points with SST below −1.8 °C have been changed to sea ice. A similar approach to generate a Heinrich event 2 like climate has been conducted by Banks et al. (2009), who lowered SST over the North Atlantic by 2 K.

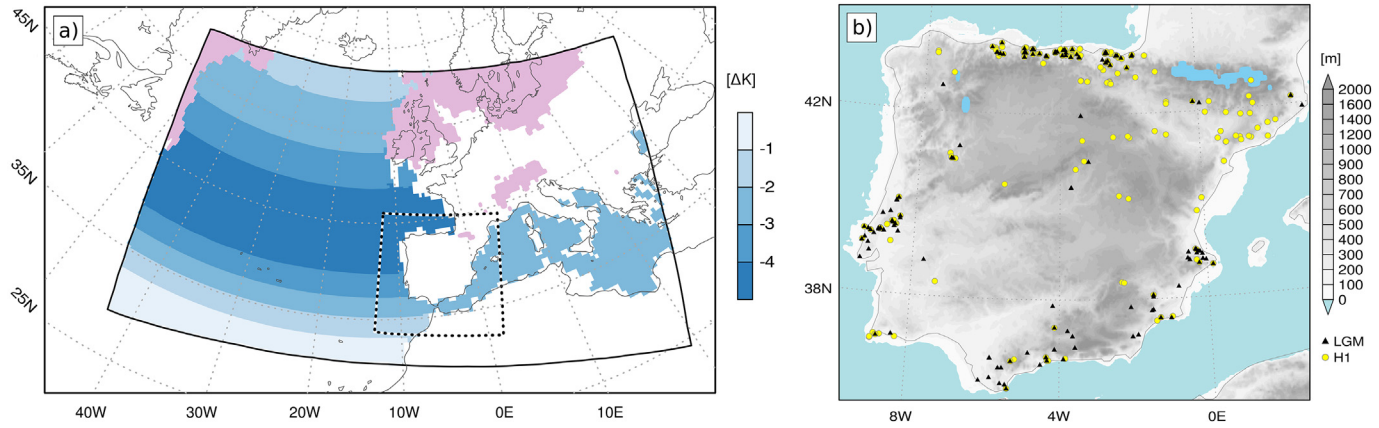

Fig. 1. (a) Model domains and imposed SST differences between WRF-H1 and WRF-LGM simulation. 50 km domain framed black, 12.5 km domain marked by black/white dashed line. Land-sea mask (including additional land area due to lowered sea level) in white; glaciers in pale red. (b) Investigation area (12.5 km model domain) with location of considered archaeological sites (LGM: black triangles; H1: yellow circles), topography (ETOPO1, Amante and Eakins, 2009) and permanent LGM/H1 ice sheets (blue) after Ehlers et al. (2011). (For interpretation of the references to colour in this figure legend, the reader is referred to the web version of this article.)

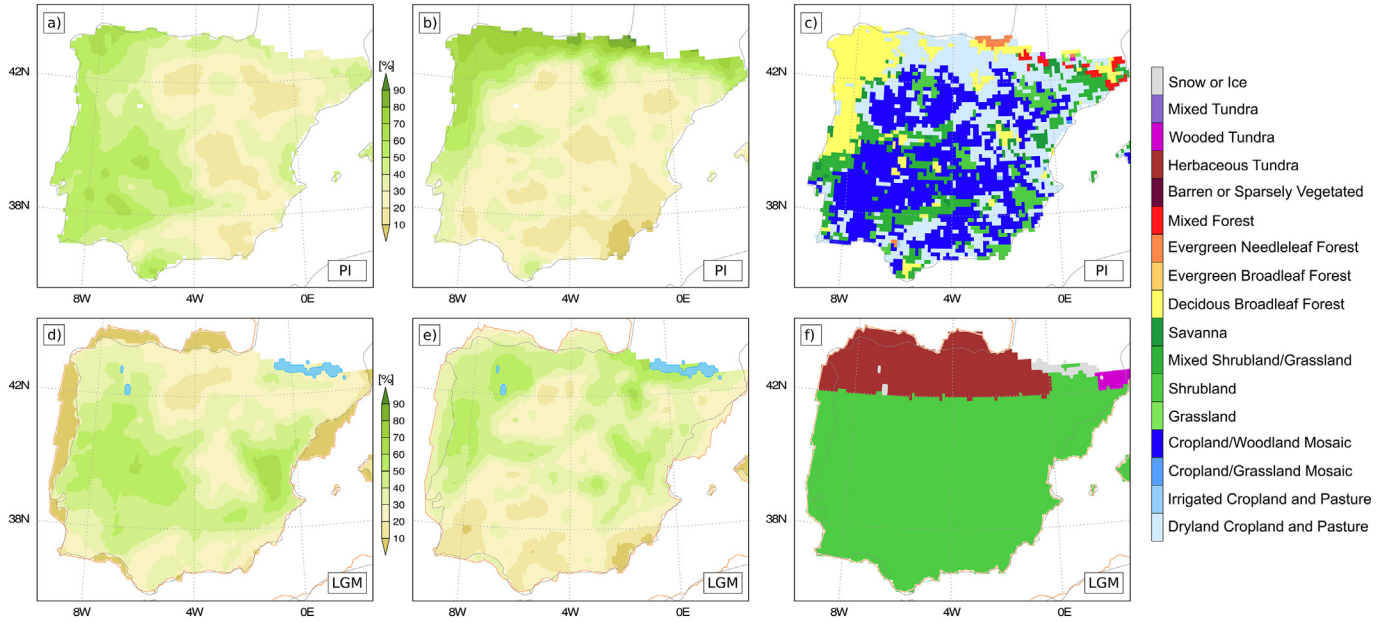

Fig. 2. Boundary conditions for regional climate simulations: vegetation cover [%] used in present day simulations for (a) January and (b) August; present day land use types (c). (d) and (e) as (a) and (b) but for glacial conditions (LGM and H1) based on CLIMAP (CLIMAP Project Members, 1984) vegetation cover reconstruction. (f) as (c) but for assumed glacial land use types also based on CLIMAP reconstructions.

Furthermore, SSTs over the Mediterranean are adjusted to the H1 climate conditions in this study. Studies by Rodrigo-Gámiz et al. (2014, and references therein) and Cacho et al. (1999) for the Alboran Sea reveal that the minima in the SST curves (cooling about 3 K) are time coincident with the Heinrich events. Results from Essallami et al. (2007) indicated that the amplitude of cooling in the central and eastern is similar to that obtained in the western Mediterranean. Based on this knowledge, a reduction of SSTs in the Mediterranean of 2.5 K was applied to the WRF simulation of the H1. Here, we use the same WRF version (version 3.5.1) with an identical model setup, including the updates for the greenhouse gas concentrations, orbital parameters, lowered sea level, and increased ice sheets as in Ludwig et al. (2017). Landuse and vegetation cover are adjusted to glacial conditions based on the CLIMAP data (CLIMAP Project Members, 1984) and kept constant for the LGM and H1 simulations (Fig. 2). Thus, differences between the LGM and H1 results are constrained to SST changes over the North Atlantic and Mediterranean and can be considered as a sensitivity experiment to changes in SST over the North-Atlantic and Mediterranean.

The simulated PI precipitation shows some typical bias compared to observations e.g., the occurrence of too many wet days with low-intensity rain (not shown) as also reported in Teutschbein and Seibert (2012). Hence, the simulated precipitation on the 12.5 km grid is corrected with the quantile-mapping approach (qmap function in R, Gudmundsson et al., 2012). For comparison and quantile-mapping, gridded precipitation datasets for Spain (Spain02, Herrera et al., 2012) and Portugal (PT02, Belo-Pereira et al., 2011) are combined and interpolated to the WRF model grid. The order of magnitude and spatial distribution of the mean annual temperature and bias-corrected precipitation for PI are compared with climatological data of Iberia provided by the Iberian Climate Atlas (AEMET-IM, 2011).

In this study, we use the aridity index (AI, UNEP, 1992) as a numerical indicator to identify regions that suffer from a deficit of available water. The AI is defined as the ratio

Table 1
Threshold values of the aridity index (AI) based on the potential evaporation and average annual precipitation and its climate classification.

Climate class	Aridity index (AI)
Hyper-arid	< 0.03
Arid	0.03–0.2
Semi-arid	0.2–0.5
Dry subhumid	0.5–0.65
Humid	> 0.65

$$AI = \frac{MAP}{PET}$$

where MAP is mean annual precipitation, and PET the annual potential evapotranspiration (see Table 1 for climate classification based on AI).

Ombrotypes are calculated under the different (palaeo-)climate conditions to quantify the environmental conditions based on temperature and precipitation (Rivas-Martínez et al., 2011). The annual and seasonal ombrothermic index (Io) is calculated as follows:

$$Io = (Pp/Tp) \times 10$$

where Tp is the positive annual temperature (total in tenths of degrees of centigrade of the average monthly temperatures higher than 0 °C, $\Sigma T_{1-12} > 0$ °C) and Pp is the positive annual precipitation (of the months with a $T_i > 0$ °C). The seasonal ombrothermic index is calculated considering the corresponding months (DJF for winter, MAM for spring, JJA for summer and SON for autumn). The resulting ombrothermic index is then assigned to an ombrotype, providing information of the state of arid/humid conditions (Table 2).

The reconstruction of the potential vegetation has been carried out based on a statistical approach after Shao et al. (2018). Here, the annual mean temperature and precipitation is used to reconstruct the distribution of 11 vegetation types in Iberia for PI, LGM and H1 climate conditions. The approach also considers the impact of the changing CO_2 concentration between PI and glacial conditions. The reconstructed vegetation types are either categorized as arboreal vegetation types (evergreen/deciduous needleleaf/evergreen forest, mixed forest, woodland and wooded grassland), non-arboreal vegetation types (closed/open shrubland, grassland) or bare ground.

Eventually, the probability of human existence for LGM and H1 conditions is estimated based on logistic regression models, a method that has already been applied in studies combining environmental and archaeological data (e.g. Burke et al., 2014; Maier et al., 2016). The Solutrean- and Magdalenian-dated archaeological sites are linked to a (sub-) set of 9 different environmental parameters for LGM and H1 including mean annual temperature (MAT), mean annual precipitation (MAP), elevation (ELV), distance of sites to coast (DC), aridity index (AI), annual ombrothermic index (Io), summer (JJA) ombrothermic index (Io3), interannual rainfall variability (RRstd) and interannual summer (JJA) rainfall variability (RRstd3). Preference scores, that are used for the logistic regression, are calculated based on probability density functions (PDF) for each environmental parameter (cf. Maier et al., 2016) to define the boundaries and optimal values of potential human existence. Grid points with scores outside of the boundaries are used as (pseudo-) absences of human existence. MAT is approximated by a Gaussian distribution, all other variables by a Weibull distribution. Different combinations of environmental parameters are tested to find the model that establishes the best linkage between the predictors and the spatial distribution of hunter-gatherer populations, based on the Akaike Information Criterion (AIC, Burnham and Anderson, 2003). The accuracy of the models to predict occupied sites / absences is validated for each model using the receiver operator curve (ROC) and the associated metric, area under the curve (AUC) as introduced by Sing et al. (2005). Each validation is based on a comparison of 100 random sets of different training (80% of the full data) and test data (remaining 20% of the full data). Finally, all individual predictors of a model have to be statistically significant to consider the model as suitable. The ROC analysis was undertaken using the ROCR package in R and the logistic regression was performed using the generalized linear model (glm) function provided by the stats package in R (R Core Team, 2017).

Table 2
Threshold values of the ombrothermic index (Io) and associated ombrotypes (including abbreviations) on the Iberian Peninsula after Rivas-Martinez et al. (2011).

	Ombrotype	Abbreviation	Io
1	Ultrahyperarid	uha	0.0–0.2
2	Hyperarid	ha	0.2–0.4
3	Arid	ar	0.4–1.0
4	Semiarid	sa	1.0–2.0
5	Dry	dr	2.0–3.6
6	Subhumid	shu	3.6–6.0
7	Humid	hu	6.0–12.0
8	Hyperhumid	hh	12.0–24.0
9	Ultrahyperhumid	uhu	> 24.0

3. Results and discussion

The outputs of the WRF simulations for PI, LGM and H1 are first validated against available climate or proxy data. Afterwards, changes in climate conditions between LGM and H1 are discussed and put into context with potential human refuges for the different time slices.

3.1. Mean PI climate conditions

The mean annual temperature (MAT) and mean annual precipitation (MAP) of the PI simulations are first validated. The overall PI temperature pattern corresponds well to the observed climate (AEMET-IM, 2011, their Fig. 5), with the warmest temperatures simulated in Andalusia and Murcia and coldest temperatures at the mountain ranges, e.g., of Sierra Nevada, Cantabrian Mountains and Pyrenees (Fig. 3a). Likewise, the magnitudes of observed and simulated MAT are similar for warm (Seville (37.4 N 5.9 W; AEMET: 18.6 °C / PI: 19.0 °C), Almeria (36.8 N 2.4 W; 18.7 °C / 18.5 °C), Lisbon (38.8 N 9.2 W; 17.0 °C / 15.8 °C)) as well as for cold locations (Burgos (42.4 N 3.6 W; 10.2 °C / 10.3 °C), Montalegre (41.8 N 7.8 W; 10.0 °C / 10.3 °C)).

The simulated PI precipitation pattern also corresponds well to the observed climate (AEMET-IM, 2011, their Fig. 69). The MAP shows a clear northwest to southeast gradient with humid conditions along the northern and western Atlantic coast (Vigo (42.2 N 8.6 W; AEMET: 1920 mm / PI: 1836 mm), San Sebastian (43.3 N 2.0 W; 1565 mm / 1681 mm)) and dry conditions along the southeastern Mediterranean coast (Alicante (38.4 N 0.5 W; 336 mm / 225 mm), Almeria (36.8 N 2.4 W; 196 mm / 163 mm)). Since the model provides reasonable results for recent climate conditions, we assume that its application to palaeo-climate conditions is suitable.

3.2. Mean LGM climate conditions

The simulated MAT reveals cold climate conditions over Iberia during the LGM (Fig. 3b). Compared to PI, the MAT along the northern and western coast of Iberia was about 2–3 K colder and up to 6 K colder in the eastern parts (Fig. 3d). The differences of LGM and PI MAT are all over significant (95% confidence interval) based on a two-sided Student's *t*-test. Proxy data from Bartlein et al. (2011) are in good agreement with the simulated MAT for southeastern Iberia, where a cooling between PI and LGM of 7.1 K is derived from pollen data. In contrast, the simulated cooling for northwestern Iberia is underestimated compared to proxy data reconstructions of 8.3 K (Bartlein et al., 2011). The distinct west-east gradient of the temperature decrease indicates the influence of warmer and moister maritime air masses at the western

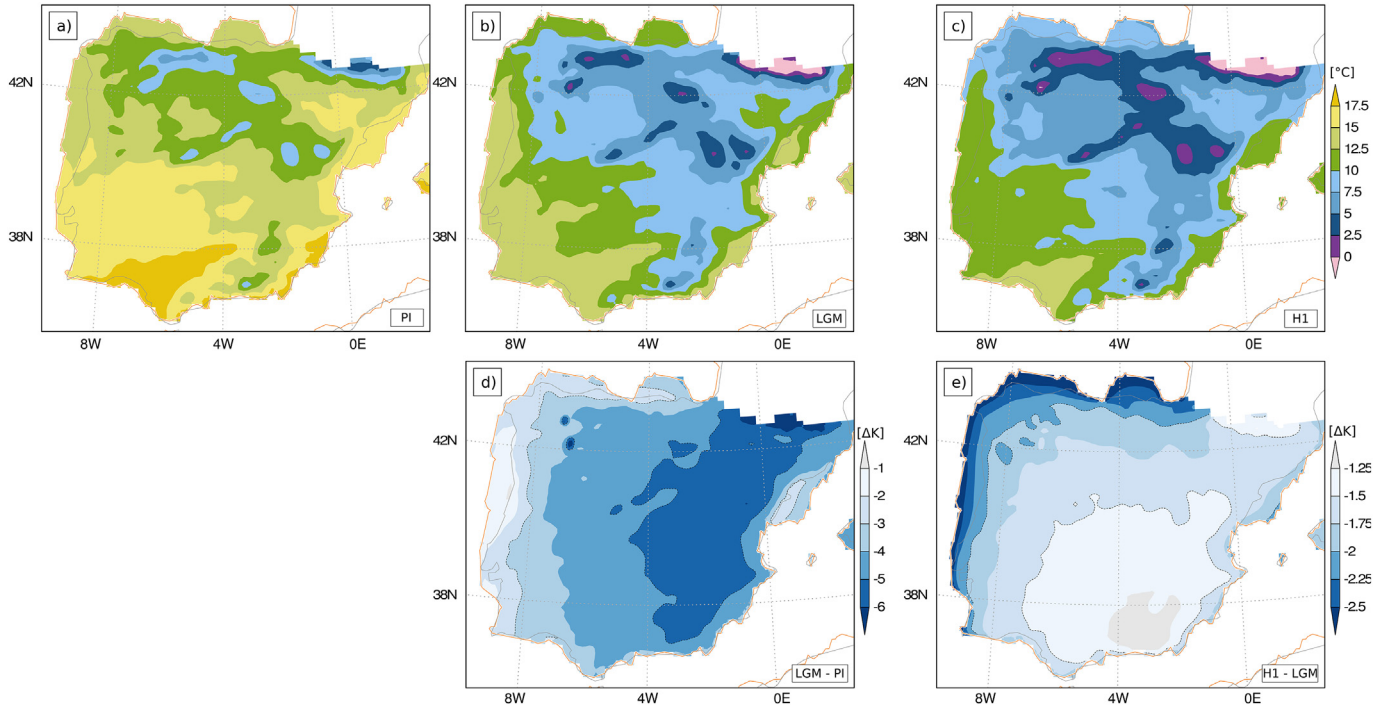

Fig. 3. Mean annual temperature [°C] as simulated by (a) WRF-PI, (b) WRF-LGM and (c) WRF-H1. (d) shows temperature difference [K] between WRF-LGM and WRF-PI, (d) between WRF-H1 and WRF-LGM.

parts of Iberia. As discussed in Ludwig et al. (2017), a warm SST anomaly over the North Atlantic in the forcing MPI-ESM-P data potentially contributes to the underestimation of cooling in northwestern parts of Iberia.

For precipitation (Fig. 4b), a significant (95% confidence interval) decrease in MAP of up to 500 mm is simulated over northwestern Iberia and the Basque Country and between 100 and 200 mm over central parts of Iberia (Fig. 4d). The simulated LGM MAP over the southern and eastern parts of Iberia is roughly equal to that in PI. The overall decrease of MAP over Iberia during LGM compared to PI amounts to 16%, with the strongest up to 50% along the slopes of the Iberian System. For the northern parts, the amount of simulated precipitation decrease is consistent with the proxy data of Bartlein et al. (2011), where the reconstructed difference between the LGM and PI amounts to 653 mm for northwestern and 500 mm for northeastern Iberia. For southeastern Iberia, the proxy reconstruction suggests a reduction of 96 mm in MAP for the LGM conditions, but this is not reproduced in our model simulations. This could be explained by the warm bias in SSTs over the Mediterranean in the forcing MPI-ESM-P data (Ludwig et al., 2017). Generally dry conditions over Iberia during the LGM are also found in other continental climate archives, e.g., speleothems (El Pindal cave, Moreno et al., 2010) and lake sediments (Padul Basin, Ortiz et al., 2010; Estanya, Morellón et al., 2009). The reduction in moisture is, for instance, clearly documented by increased percentages of semi-desert taxa (Artemisia, Chenopodiaceae, *Ephedra distachya* etc., Carrión et al., 2010) and steppe vs. forest vegetation in pollen records of Padul (Pons and Reille, 1988) and the Alborán Sea (MD95-2043, Fletcher and Sánchez Goñi, 2008; ODP976, Combourieu Nebout et al., 2009). Dry climatic conditions may also be deduced from formation of clay dunes in the Manchega Plain, dated between 28 and 18 ka (Bernat Rebollal and Pérez-González, 2008). The $d^{18}O$-speleothem record of Eagle cave, located in Central Iberia suggests that the LGM was drier than the end of MIS3, when Iberian glaciers reached maximum extent (Domínguez-Villar et al., 2013). The same record show peaks in less negative values indicating aridity for H2 (and H3). It should be noted, however, that pollen records of core MD95-2042 retrieved from the Iberian shelf off southern Portugal suggest that the LGM was less cold and dry than the end of MIS3 or than stadial periods correlating with Heinrich events (Roucoux et al., 2005). The lake level data from Fuentillejo maar (Vegas et al., 2010) suggest also an increase of lake level during the LGM. Since the lake is considered as a closed system, the lake level is associated with the balance of precipitation and evaporation (Beghin et al., 2016). Thus, high lake level may not be associated with higher precipitation but with reduced evaporation due to lower temperatures during LGM compared to PI (Prentice et al., 1992). This fact could also be used to explain the contradictory results obtained from pollen and lake level data e.g. at lake La Salineta in the Ebro valley (Valero-Garcés et al., 2004). Here, pollen sequences suggest dry conditions (steppe species) while geochemical and sedimentary analysis from lake records indicate enhanced moisture.

3.3. Mean H1 climate conditions

The simulated mean climate conditions for the H1 event reveal colder (Fig. 3 c, e) and drier (Fig. 4 c, e, g) conditions in Iberia than for the LGM. The reduced SSTs during H1 cause a strong drop in temperature along the western and northern Atlantic coast of up to 3.3 K and a moderate decline in southeastern parts of 1 K (Fig. 3e). Iberia experienced an overall significantly (95% confidence interval) reduced MAT of 1.7 K compared to the LGM conditions. The results for MAT are partly similar to those obtained by Kageyama et al. (2005). In their simulation, the strongest temperature decrease also occurs along coastal areas exposed to the Atlantic Ocean. In contrast, their results did not show any temperature decrease in the southeastern parts of Iberia, as in their simulation, the SST over the Mediterranean was the same as for the LGM.

The absolute reduction of precipitation from LGM to H1 is strongest along the northern Iberian coast, causing a reduction of MAP of up to 400 mm. Except for some scattered spots and a coherent area in Catalonia, the decrease in MAP is significant (95% confidence interval). On average, the reduction of MAP over Iberia is 114 mm (relative 20%) compared to the LGM climate. The strongest relative decrease of MAP (up to 40%) based on our simulation can be observed along the southeastern coast and is contrary to the results from Kageyama et al.

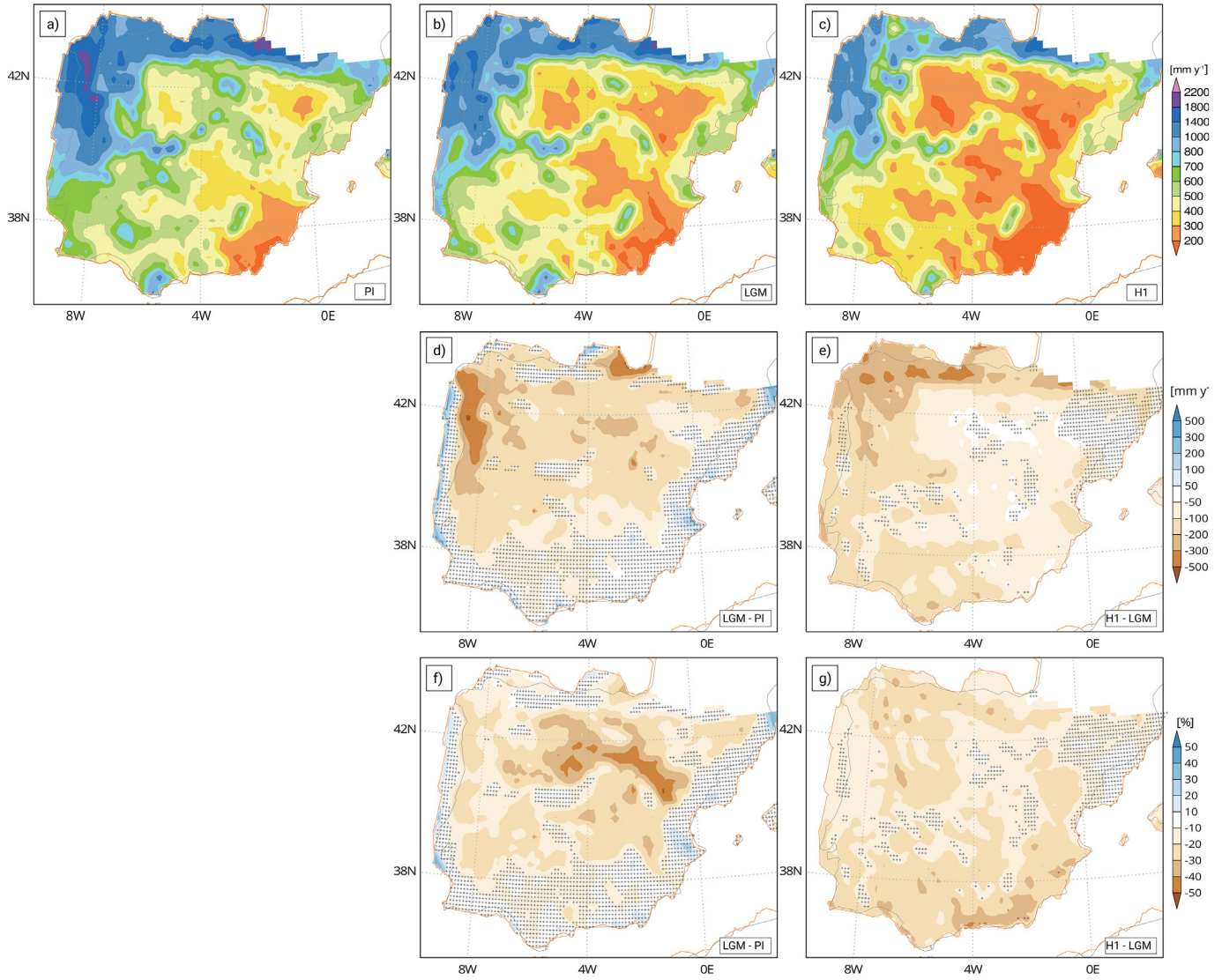

Fig. 4. Mean annual precipitation [mm y^{-1}] for (a) WRF-PI, (b) WRF-LGM and (c) WRF-H1 simulation. (d) absolute precipitation difference [mm y^{-1}] between WRF-LGM and WRF-PI, (e) between WRF-H1 and WRF-LGM. (f) and (g) same as (d) and (e) but for relative precipitation differences. Non-significant changes (two-sided Student's *t*-test, 95% confidence interval) indicated by hatched areas.

(2005), who simulated increased precipitation over southeastern parts of Iberia for H1. This demonstrates the importance of a comprehensive adaption of boundary conditions when simulating the regional palaeoclimate, e.g. the additional adjustment of Mediterranean SST made in this study. Kageyama et al. (2005) already noted this point in their study.

The continental proxy data suggest that the H1 was colder and drier compared to the LGM in Iberia (Moreno et al., 2012 and references therein), which support our model results. In marine cores from the Iberian shelf, H1 is characterized by maxima of the cold-water foraminifer *Neoglobigerina pachyderma (s)* and in ice rafted debris (IRD) while those of the Alborán Sea show peaks in cold water foraminifers only. Concomitantly, minima in reconstructed SST, for instance, in core ODP976 of the Alborán Sea (Martrat et al., 2014), and increases in cold- or arid-tolerant pollen are observed. Interestingly, pollen spectra for H1 both in the marine cores off NW-Iberia (Naughton et al., 2016) and in the Alborán Sea (Fletcher and Sánchez Goñi, 2008) show a tripartite pattern with maximum dryness during the second phase lasting for about 1500 years. Some records from the Cantabrian Mountains and the Pyrenees show a two-phase pattern for H1 (Jalut et al., 2010) while a single cold and dry phase was reported from El Portalet sequence (González-Sampériz et al., 2006).

After H1, Greenland Interstadial 1 was a phase of climate amelioration, well represented in pollen spectra, reconstructed SST and other climate proxies. At Padul (Pons and Reille, 1988), it is characterized by a clear spread of Quercus type pollen and a reduction in Artemisia, reflecting a regional climatic pattern, which is closely mirrored in the MD95-2043 core (Fletcher and Sánchez Goñi, 2008).

3.4. Climate change, palaeoenvironment and population dynamics

We now discuss the link between climatic changes, palaeovegetation and human settlement patterns. As shown before, the climate over Iberia was (significantly) colder and drier in H1 than in LGM. Since the archaeological evidence for the LGM and H1 shows sparse population of the South during H1 (Fig. 1b), the focus is particularly on the different climate conditions in southern Iberia. Fig. 5 shows the aridity index (AI, UNEP, 1992) based on the WRF-LGM and WRF-H1 simulation. For LGM and H1, the AI shows a northwest to southeast gradient with humid conditions in northwestern and arid conditions in southeastern Iberia. During H1, the AI indicates more arid conditions compared to LGM (Fig. 5c), which is particularly true along the southeastern

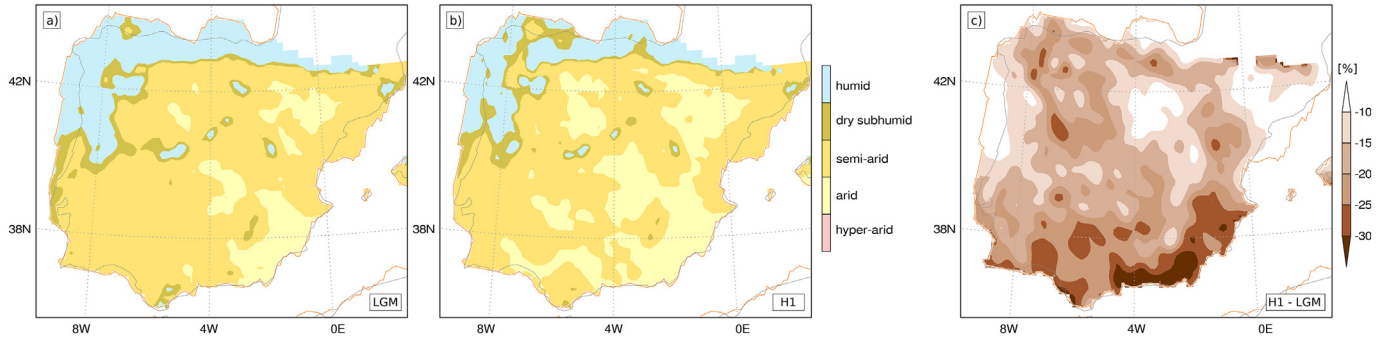

Fig. 5. Aridity index based on (a) WRF-LGM simulation and (b) WRF-H1 simulation. (c) shows relative differences of the aridity index in [%] where brownish colours indicate more arid conditions during H1.

Mediterranean coast. While humans apparently occupied this area during the LGM, very few sites with occupancy remain during H1. The strongest increase in number of sites can be observed in northwestern Iberia, corresponding to a region that shows hardly any change of the AI. The consideration of the ombrotypes (Rivas-Martínez et al., 2011) confirms these results (Fig. 6). While northwestern Iberia is characterized by humid to hyper-humid conditions for PI, LGM (even more humid than PI) and H1 (Fig. 6 a-c), a shift towards more arid conditions can be observed in southeastern Iberia during H1. The relative area in Iberia covered by arid conditions increased from 0.19% for LGM to 0.73% during H1 for annual mean conditions (Fig. 7a). The area characterized by semi-arid conditions even increases from 3.0% (LGM) to 13.5% (H1). On the other hand, areas with sub-humid, humid and hyper-humid conditions decrease during H1. The most striking effect of the different climate conditions during H1 is noticeable when comparing the seasonal Io for summer (Fig. 6j–l, Fig. 7d). Here, the southern parts of Iberia are clearly affected by extremely dry conditions, indicated by an increase of areas assigned with a hyperarid (H1: 22.7%; LGM 19.5%) and particularly ultrahyperarid Io (H1: 22.6%; LGM: 2.1%). The generally drier conditions during H1 in southern Iberia are also derived from the proxy data from Padul (n-Alkane: Ortiz et al., 2010). During the transitional seasons (spring: Fig. 6d-f, Fig. 7c; autumn: Fig. 6m–o, Fig. 7e) the differences of the spatial and relative distributions of the Io are rather small, thus emphasizing the importance of the summer season drought conditions on the inhabitability of southern Iberia.

The distribution of occupied sites found for LGM and H1 indicates that regions with subhumid and humid conditions are preferred for habitability (Fig. 7f). For H1, the majority of the sites (58%) are found in the subhumid and humid area and for LGM the ratio is even 67%. An increase of sites found in dry conditions is noticeable for H1 (23% vs. 13% for LGM, Fig. 7f), pointing towards a certain ability of human adaption towards drier conditions.

To consider the effects of the different climate conditions on the palaeovegetation, the results of the reconstruction of the potential vegetation after Shao et al. (2018) in Iberia is shown in Fig. 8. A clear decrease of arboreal vegetation types is reconstructed as a consequence of the different climate conditions between PI and LGM (Fig. 8 a,b). During H1, the arboreal types further decrease and their potential existence is limited to northwestern parts of Iberia, with only a few patches of arboreal vegetation remaining in the south and over mountainous areas in central Iberia (Fig. 8c). In contrast, the reconstructed non-arboreal vegetation ratio increases from PI to LGM and H1 (Fig. 8 d-f). Especially in central and southern Iberia exhibits an increase of more open vegetation (open shrubland, grassland) pointing towards a more steppe-like vegetation during glacial and in particular for H1 conditions. This is also supported by an increased amount of bare ground, which is highest for the H1 climate conditions. These results are in good agreement with results from pollen analysis that show increased percentages of steppe vs. forest vegetation at Padul (Pons and Reille, 1988; Ortiz et al., 2010), and the Alborán Sea (MD95-2043, Fletcher and Sánchez Goñi, 2008; ODP976, Combourieu Nebout et al., 2009).

An additional analysis of the link between environmental conditions and archaeological sites is carried out by means of a logistic regression analysis. For that, the considered environmental parameters mean annual temperature (MAT), mean annual precipitation (MAP), elevation (ELV), distance of sites to coast (DC), aridity index (AI), annual ombrothermic index (Io), summer (JJA) ombrothermic index (Io3), interannual rainfall variability (RRstd) and interannual summer (JJA) rainfall variability (RRstd3) were selected at the grid points including the archaeological sites for both LGM and H1 conditions, respectively. The frequency distributions (Fig. 9) were approximated either by a Gaussian distribution for MAT (Fig. 9a) or a Weibull distribution for all other predictors (see Fig. 9b exemplarily for ELV). Based on the determined boundaries, different models are tested to predict human existence for LGM and H1. The boundaries (lower: 5% quantile, upper: 95% quantile) for the final set of predictors used in the logistic regression are summarized in Table 3. The best performing models determined by AUC (an AUC of 0.85 indicates an accuracy rate of 85% of the model predictions) include (i) MAT, RRstdJJA, ELV, Io3 (mod_1) and (ii) additionally DC (mod_2) as statistically significant predictors (see Table 4 for estimates and model performance). Fig. 10 shows the resulting potential for human existence based on the two best performing models for LGM and H1 environmental conditions. During LGM, high probabilities for human occupancy existed along the Iberian coastline (Fig. 10a, c), where the Solutrean sites are grouped in three regions: (i) along the Asturias / Cantabrian coast, (ii) western Iberia (administrative division Oeste, Portugal) and along the southeastern coast. The general pattern of mod_1 agrees well with the predicted probability of occurrence of archaeological sites based on a study by Burke et al. (2014). The pattern of mod_2, including DC, agrees well with the final habitat suitability model constructed Burke et al. (2017). During H1 (Fig. 10b, d), the probability of site occurrence particularly decreases in the southern parts of Iberia. Favourable environmental conditions exist primarily in the northern parts where most of the Magdalenian sites were found. Especially the Ebro valley, which was almost uninhabited during LGM, experienced a widespread increase of dated sites. The probability along the western Iberian coast is persistently large, however the number of sites decreases during H1. In southern Iberia, only a few inhabited Magdalenian sites remain during the H1 conditions. The outcome of the potential human existence modelling agrees well with the prior described changes of environmental conditions during LGM and H1.

4. Summary and additional discussions

We investigated the human settlement patterns in Iberia for LGM and H1 environmental conditions based on archaeological archives and high-resolution climate model data. The WRF model is used to obtain a 30-year time slice of the different climate conditions in LGM and H1,

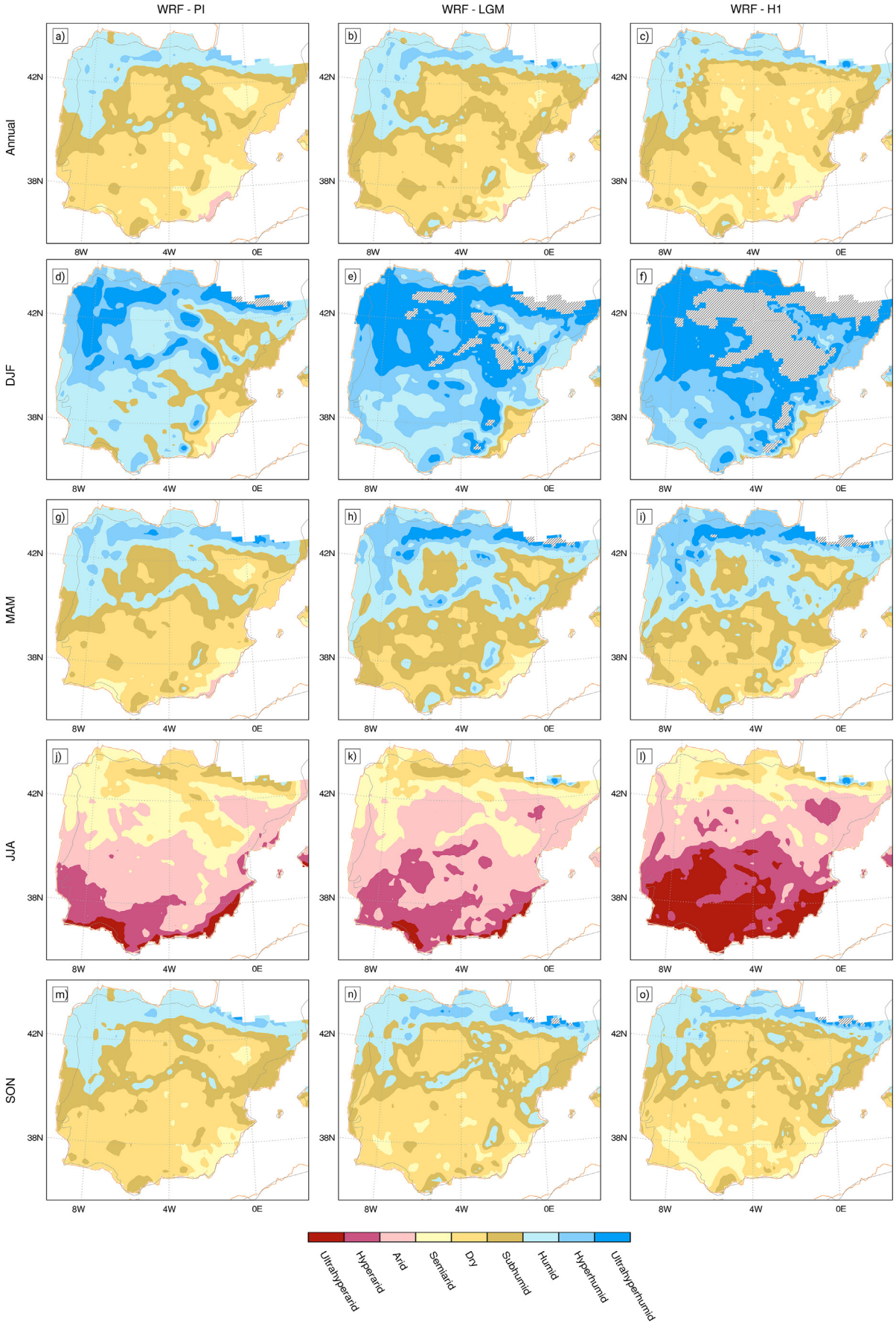

Fig. 6. Annual and seasonal ombrotypes (after Rivas-Martínez et al., 2011) based on WRF-PI, WRF-LGM and WRF-H1 simulations. Regions with no positive annual / seasonal temperatures hatched.

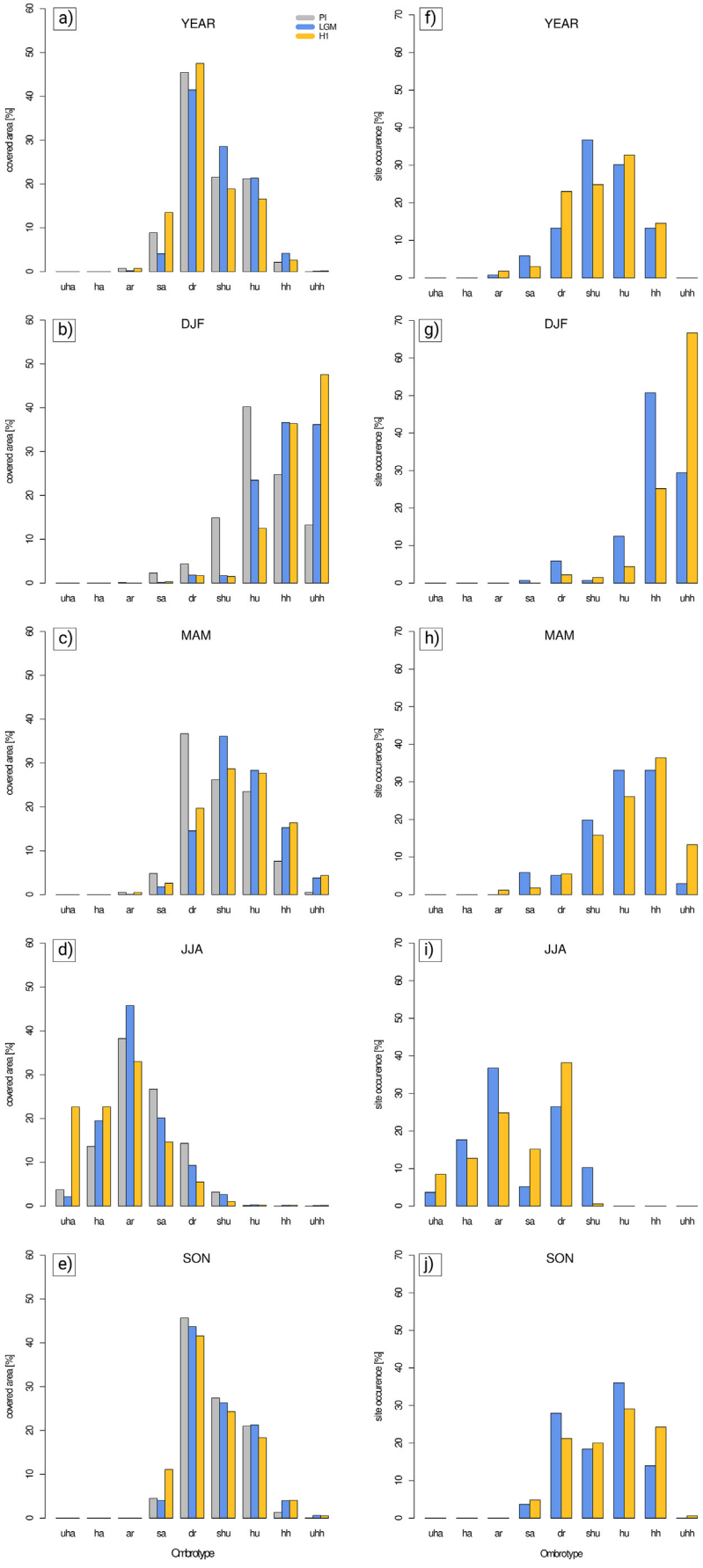

(caption on next page)

Fig. 7. Left column: annual and seasonal distribution of area in Iberia covered by ombrotype for WRF-PI (grey bars), WRF-LGM (blue bars) and WRF-H1 (yellow bars); right column: annual and seasonal distribution per ombrotype for Solutrean (blue bars) and Magdalenian (yellow bars) sites. Ombrotype classification based on Rivas-Martínez et al. (2011): (uha) ultrahyperarid, (ha) hyperarid, (ar) arid, (sa) semiarid, (dr) dry, (shu) subhumid, (hu) humid, (hh) hyperhumid, (uhh) ultra-hyperhumid. (For interpretation of the references to colour in this figure legend, the reader is referred to the web version of this article.)

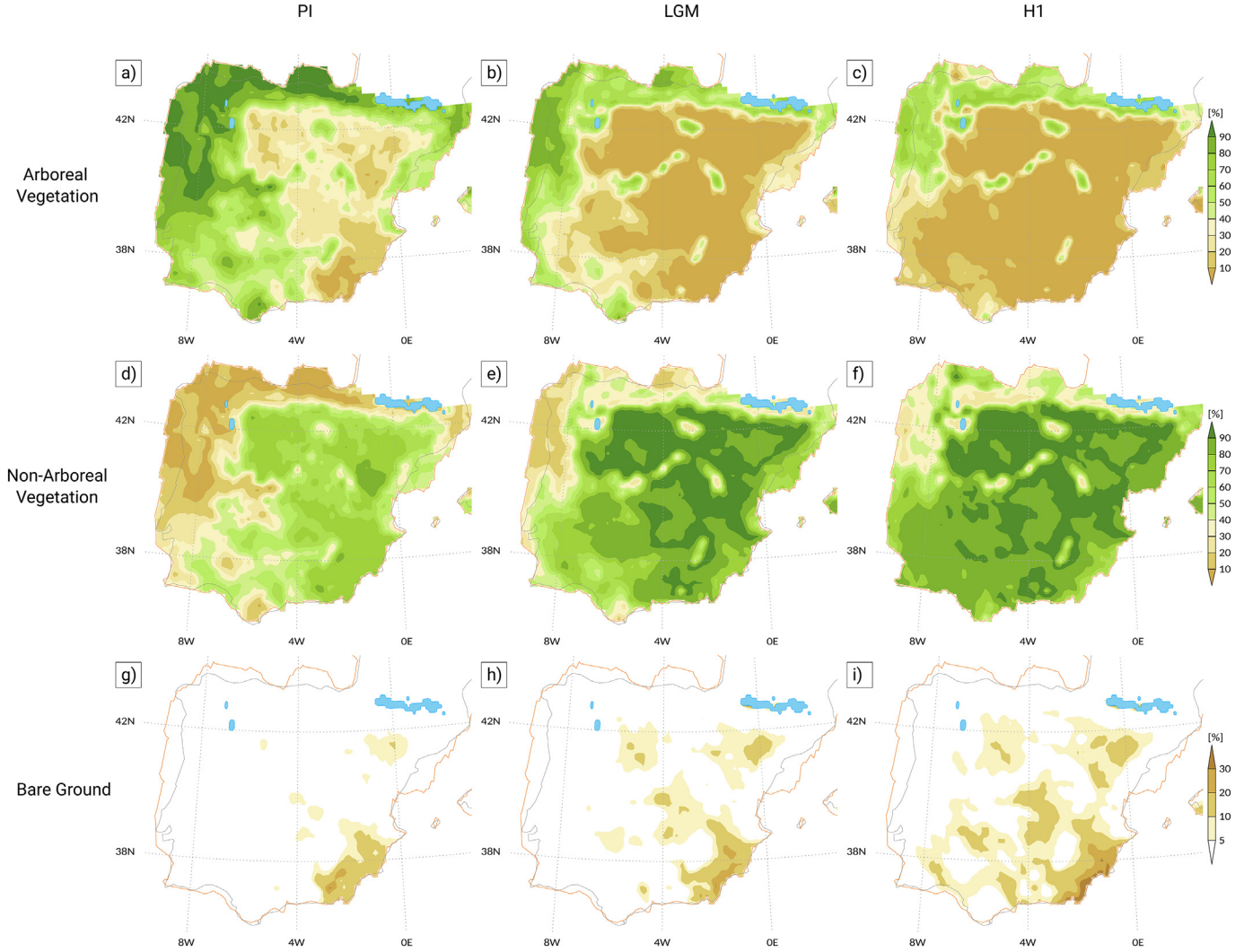

Fig. 8. Distribution of the reconstructed potential vegetation types in Iberia based on the simulated mean annual temperature and precipitation for PI, LGM and H1. Vegetation is grouped into arboreal types for (a) PI, (b) LGM (c) H1 climate conditions and non-arboreal types for (d) PI, (e) LGM, (f) H1 climate conditions. The distribution of areas featuring bare ground is also shown for (g) PI, (h) LGM and (i) H1 climate conditions.

enabling an examination of the influences of climate change on human habitation. For the H1 simulation, SSTs over the North Atlantic and Mediterranean are reduced to take into account the weakening of the meridional overturning circulation (McManus et al., 2004). The resulting simulations reveal in general colder and drier conditions during the H1 compared to the LGM, which are consistent with the proxy data (Moreno et al., 2012, and references therein). A simulation by Kageyama et al. (2005) for H1 showed a reduction of the temperature of the coldest month and precipitation, particularly on the Atlantic coast. In contrast to our results, their simulation reveal slightly increased precipitation along the Mediterranean coast in H1 compared to LGM, which is possibly due to that they neglect the decrease in Mediterranean SST in their model of. Kageyama et al. (2005) propose that imposing available Mediterranean SST reconstructions would lead to a larger impact around the Alboran Sea. Our H1 simulations, with adjusted Mediterranean SSTs (Rodrigo-Gámiz et al., 2014; Cacho et al., 1999; Essallami et al., 2007), show a (strong) reduction of precipitation over the southern / southeastern Iberia, and thereby confirm the hypothesis of Kageyama et al. (2005). In summary, the high resolution palaeoclimate simulation is capable to reproduce the different climate stages considered in this study.

Most importantly, southern Iberia exhibits drought conditions during the summer season at H1 (Fig. 6), depicted by an increase in hyperarid (H1: 22.7%; LGM 19.5%) and particularly ultrahyperarid (H1: 22.6%; LGM: 2.1%) ombrotypes (Rivas-Martínez et al., 2011). Since the other seasons show almost similar ombrothermic conditions, we assume that the changes in the summer season played the most important role in the different human settlement patterns in Iberia between the LGM and H1. A reduction of water availability during summer could cause limited growth of plants, leading to a retreat of vegetation that limits the availability of food supply like plants and animals that are reliant on these plants. For the present climate, Dietrich and Smith (2016) investigated the timing of rainfall deficit (drought) on the flowering of C4 plants (here *Andropogon gerardii*). Their results show that a mid-summer drought strongly reduced the flowering rate as high as 94% (density and biomass), providing an

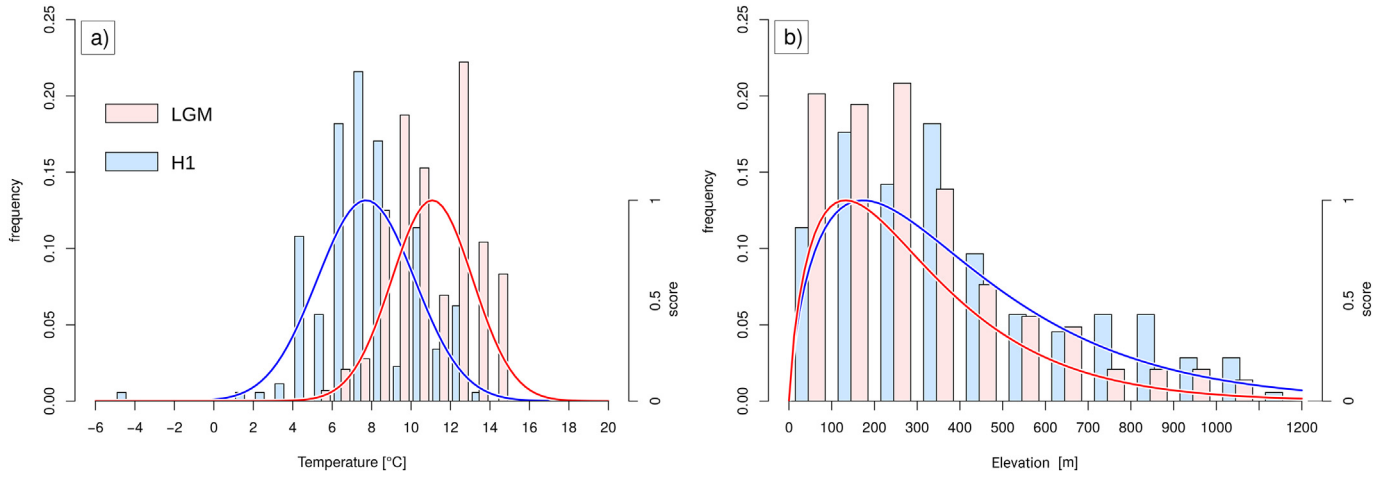

Fig. 9. Exemplary histograms of the distribution of environmental conditions at archaeological sites for LGM (red) and H1 (blue) to derive preference scores that are used for logistic regression: a) mean annual temperature (MAT) [°C] and b) elevation (ELV) [m]. The curves show the normalized fitted distributions (Gaussian distribution for MAT, Weibull distribution for ELV) used for the calculation of scores (1 – best, 0 – unfavourable environmental conditions) for each variable. (For interpretation of the references to colour in this figure legend, the reader is referred to the web version of this article.)

Table 3
Boundaries (5% – / 95% - quantile; score = 0) for human existence based on the fitted distributions for the predictors of the best models including MAT: annual mean temperature, RRstd3: standard deviation of rainfall in summer (JJA), ELV: elevation, Io3: ombrothermic index summer (JJA) and DC: distance of sites to coast (see Fig. 8 of exemplary distributions for MAT and ELV).

	MAT [°C]		RRstd3 [mm]		ELV [m]		Io3		DC [m]	
	LGM	H1	LGM	H1	LGM	H1	LGM	H1	LGM	H1
5% - quantile	7.70	3.65	10.68	10.17	38.38	50.86	0.1	0.13	2.93	4.45
95% - quantile	14.45	11.78	81.66	65.98	754.53	1004.6	4.27	3.81	162.03	215.75

Table 4
Logistic regression parameter estimates and performance of the finally selected models to predict human existence probabilities based on environmental parameters for LGM and H1 conditions. Estimate and Standard error are parameters of the logistic regression, *p*-value gives information about the statistical significance of the predictors, AIC is the Akaike Information Criterion and AUC is the resulting mean of the ROC, representing the accuracy of the model predictions.

Model	Predictors	Estimate		Standard error		p-Value		AIC		AUC	
		LGM	H1	LGM	H1	LGM	H1	LGM	H1	LGM	H1
Mod_1	(Intercept)	−7.14	−7.54	0.81	0.84			275.17	327.80	0.88	0.85
	MAT	6.12	6.67	0.59	0.63	< 0.001	< 0.001				
	RRstdJJA	2.80	5.68	1.02	0.88	0.015	< 0.001				
	ELV	6.88	6.42	0.61	0.64	< 0.001	< 0.001				
	Io3	−3.01	−4.50	0.75	0.76	< 0.001	< 0.001				
Mod_2	(Intercept)	−8.19	−8.87	0.73	0.76			398.02	474.51	0.81	0.78
	MAT	3.76	4.16	0.50	0.44	< 0.001	< 0.001				
	RRstdJJA	4.23	6.63	0.91	0.77	< 0.001	< 0.001				
	ELV	4.60	3.95	0.47	0.46	< 0.001	< 0.001				
	Io3	−5.69	−5.21	0.76	0.60	< 0.001	< 0.001				
	DC	6.92	5.28	0.58	0.51	< 0.001	< 0.001				

indication of sensitivity to precipitation. Based on Collatz et al. (1998), predominantly C4 plants were present in Iberia around the LGM. The reconstruction of the potential vegetation (Shao et al., 2018) based on the PI, LGM and H1 climate conditions supports the hypothesis of limited availability of food supply due to vegetation degradation during H1. An increase of open steppe-like vegetation (increase of non-arboreal vegetation types including (open) shrubland and grassland) at the expense of arboreal vegetation types is reconstructed for H1. Additionally, the increased amount of bare ground in southern Iberia indicates a desertification during the H1 period. Similar results for changes in palaeovegetation (shift from arboreal to non-arboreal vegetation, desertification in southern Iberia) are obtained by Sepulchre et al. (2007) for a different Heinrich stadial (H4). It appears that particularly southern Iberia is subjected to drastic environmental changes during the cold and dry climate conditions of Heinrich Events. Proxy-data based analyses of variations of the vegetation under H1 conditions also reflect the accompanied cold and dry climate. Based on n-alkanes, a drastic retreat of tree species (C_{27}) and spread of non-arboreal plants (C_{31}) is reconstructed at the Padul Basin (southern Iberia; Ortiz et al., 2010, their Fig. 6). Furthermore, pollen sequences from marine cores in the realm of southern Iberia reveal a shift to steppe taxa during the H1 interval (Fletcher and Sánchez Goñi, 2008, Fletcher et al., 2010, their Fig. 3). The climatic changes from LGM to H1 did not cause a gap in human occupation in the North, which is consistent with the prediction of the probability of human existence based on results from logistic regression. Possible explanations for this may be that the ecosystems had higher resilience against climate change.

The application of high resolution climate simulations enables to

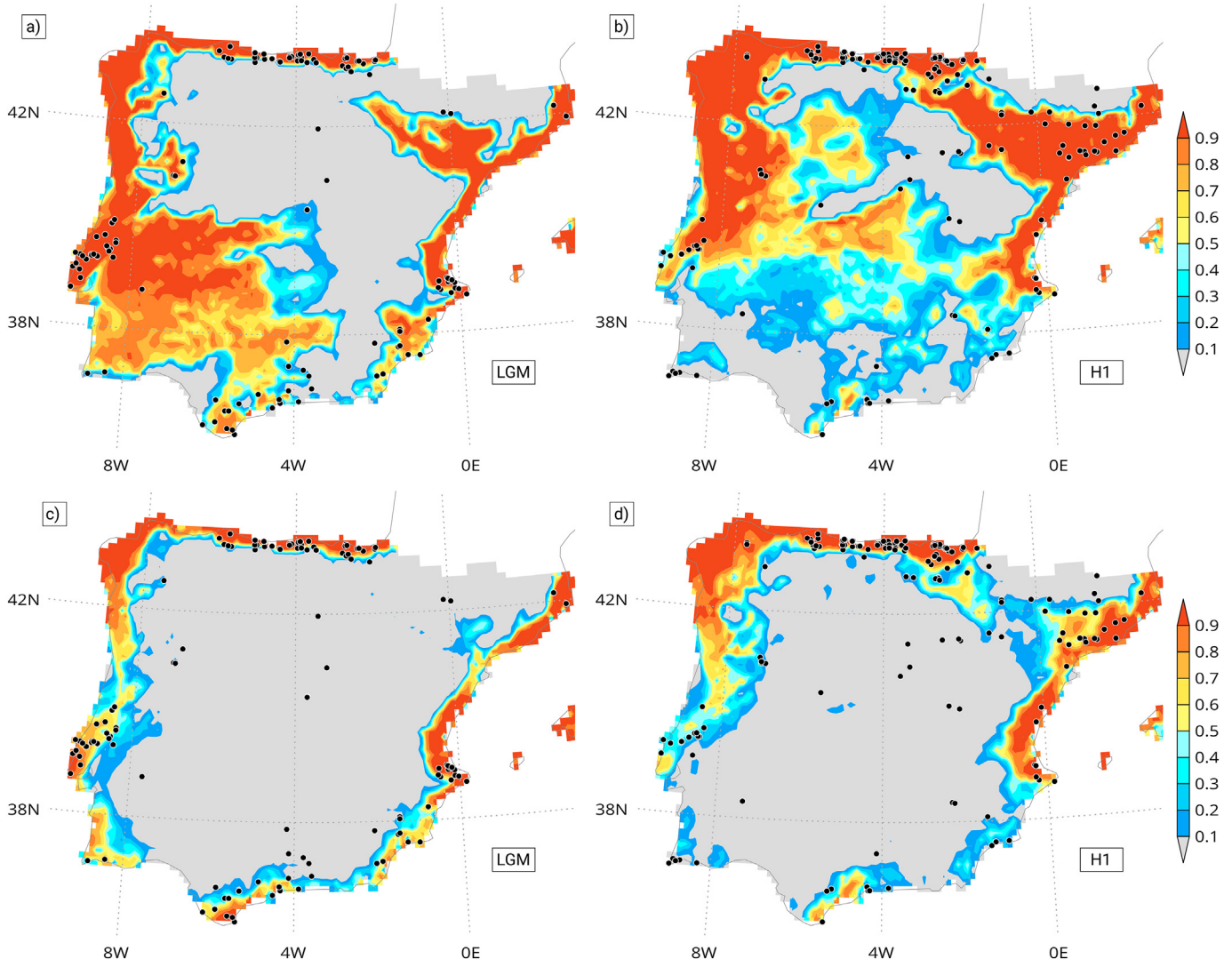

Fig. 10. Probability of site occurrence based on the best performing logistic regression models with 4 environmental predictors (MAT, ELV, RRstd3, Io3) for a) WRF-LGM and Solutrean sites, b) for WRF-H1 and Magdalenian sites. (c) and (d) as (a) and (b) but with additional predictor DC.

trace high-frequency climate variations that do not show up in coarse scale grid simulations (Tallavaara et al., 2015). Likewise, their simulated population density over Iberia differs from our findings and results from studies by Burke et al. (2014, 2017) and from eco-cultural niche modelling studies by Banks et al. (2008). In Tallavaara et al. (2015), high population densities for LGM were calculated particularly along the southern Iberian coast, while low population densities (and thus unfavourable environmental conditions) were assumed along the northern Iberian coast. However, the predicted probability of occurrence of archaeological sites during LGM in our study agrees well with results from Burke et al. (2014, 2017) and Banks et al. (2008), revealing favourable conditions for the presence of Solutrean populations along the northern and eastern Iberian coast.

Acknowledgments

We thank the German Climate Computing Centre (DKRZ, Hamburg) for providing the computing resources (project 965). The authors acknowledge financial support by the German Research Foundation (DFG) (SFB 806) through projects E6 and C1 of the CRC 806 (Our Way to Europe). We thank Joaquim Pinto (Karlsruhe Institute of Technology) for discussions. We thank two anonymous reviewers for providing very helpful comments that improved this article. All Data and software are available on request from the authors (patrick.ludwig@kit.edu).

References

AEMET-IM, 2011. Iberian Climate Atlas. Agencia Estatal de Meteorología (España) and Instituto de Meteorología (Portugal), Madrid, Spain.

Álvarez-Solas, J., Montoya, M., Ritz, C., Ramstein, G., Charbit, S., Dumas, C., Nisancioglu, K., Dokken, T., Ganopolski, A., 2011. Heinrich event 1: an example of dynamical ice-sheet reaction to oceanic changes. Clim. Past 7, 1297–1306. https://doi.org/10.5194/cp-7-1297-2011.

Amante, C., Eakins, B.W., 2009. ETOPO1 1 Arc-Minute Global Relief Model: Procedures, Data Sources and Analysis. NOAA Technical Memorandum NESDIS NGDC-24. Retrieved from. http://www.ngdc.noaa.gov/mgg/global/global.html.

Banks, W.E., D'Errico, F., Peterson, A.T., Vanhaeren, M., Kageyama, M., Sepulchre, P., Ramstein, G., Jost, A., Lunt, D., 2008. Human ecological niches and ranges during the LGM in Europe derived from an application of eco-cultural niche modeling. J. Archaeol. Sci. 35, 481–491. https://doi.org/10.1016/j.jas.2007.05.011.

Banks, W.E., Zilhão, J., D'Errico, F., Kageyama, M., Sima, A., Ronchitelli, A., 2009. Investigating links between ecology and bifacial tool types in Western Europe during the last glacial maximum. J. Archaeol. Sci. 36, 2853–2867. https://doi.org/10.1016/j.jas.2009.09.014.

Bartlein, P.J., Harrison, S.P., Brewer, S., Connor, S., Davis, B.A.S., Gajewski, K., Guiot, J., Harrison-Prentice, T.I., Henderson, A., Peyron, O., Prentice, I.C., Scholze, M., Seppä, H., Shuman, B., Sugita, S., Thompson, R.S., Viau, A.E., Williams, J., Wu, H., 2011. Pollen-based continental climate reconstructions at 6 and 21 ka: a global synthesis. Clim. Dyn. 37, 775–802. https://doi.org/10.1007/s00382-010-0904-1.

Beghin, P., Charbit, S., Kageyama, M., Combourieu-Nebout, N., Hatté, C., Dumas, C., Peterschmitt, J.Y., 2016. What drives LGM precipitation over the western

Mediterranean? A study focused on the Iberian Peninsula and northern Morocco. Clim. Dyn. 46, 2611–2631. https://doi.org/10.1007/s00382-015-2720-0.
Belo-Pereira, M., Dutra, E., Viterbo, P., 2011. Evaluation of global precipitation data sets over the Iberian Peninsula. J. Geophys. Res. 116, D20101. https://doi.org/10.1029/2010JD015481.
Bernat Rebollal, M., Pérez-González, A., 2008. Inland aeolian deposits of the Iberian Peninsula: sand dunes and clay dunes of the Duero Basin and the Manchega plain. Palaeoclimatic considerations. Geomorphology 102, 207–220. https://doi.org/10.1016/j.geomorph.2008.05.009.
Braconnot, P., Harrison, S.P., Kageyama, M., Bartlein, P.J., Masson-Delmotte, V., Abe-Ouchi, A., Otto-Bliesner, B., Zhao, Y., 2012. Evaluation of climate models using palaeoclimatic data. Nat. Clim. Chang. 2, 417–424. Retrieved from. https://doi.org/10.1038/nclimate1456.
Bradtmöller, M., Pastoors, A., Weninger, B., Weniger, G.C., 2012. The repeated replacement model - rapid climate change and population dynamics in late Pleistocene Europe. Quat. Int. 247, 38–49. https://doi.org/10.1016/j.quaint.2010.10.015.
Burke, A., Levavasseur, G., James, P.M.A., Guiducci, D., Izquierdo, M.A., Bourgeon, L., Kageyama, M., Ramstein, G., Vrac, M., 2014. Exploring the impact of climate variability during the last glacial maximum on the pattern of human occupation of Iberia. J. Hum. Evol. 73, 35–46. https://doi.org/10.1016/j.jhevol.2014.06.003.
Burke, A., Kageyama, M., Latombe, G., Fasel, M., Vrac, M., Ramstein, G., James, P.M.A., 2017. Risky business: the impact of climate and climate variability on human population dynamics in Western Europe during the last glacial maximum. Quat. Sci. Rev. 164, 217–229. https://doi.org/10.1016/j.quascirev.2017.04.001.
Burnham, K.P., Anderson, D.R., 2003. Model Selection and Multimodel Inference: A Practical Information-theoretic Approach. Springer, New York.
Cacho, I., Grimalt, J.O., Pelejero, C., Canals, M., Sierro, F.J., Flores, J.A., Shackleton, N., 1999. Dansgaard-Oeschger and Heinrich event imprints in Alboran Sea paleotemperatures. Paleoceanography 14, 698–705. https://doi.org/10.1029/1999PA900044.
Carrión, J.S., Fernández, S., González-Sampériz, P., Gil-Romera, G., Badal, E., Carrión-Marco, Y., López-Merino, L., López-Sáez, J.A., Fierro, E., Burjachs, F., 2010. Expected trends and surprises in the Lateglacial and Holocene vegetation history of the Iberian Peninsula and Balearic Islands. Rev. Palaeobot. Palynol. 162, 458–475. https://doi.org/10.1016/j.revpalbo.2009.12.007.
CLIMAP Project Members, Ruddiman, W.F., Cline, R.M.L., Hays, J.D., Prell, W.L., Ruddiman, W.F., Moore, T.C., Kipp, N.G., Molfino, B.E., Denton, G.H., Hughes, T.J., Balsam, W.L., Brunner, C.A., Duplessy, J.C., Fastook, J.L., Imbrie, J., Keigwin, L.D., Kellogg, T.B., McIntyre, A., Matthews, R.K., Mix, A.C., Morley, J.J., Shackleton, N.J., Streeter, S.S., Thompson, P.R., 1984. The last interglacial ocean. Quat. Res. 21, 123–224. https://doi.org/10.1016/0033-5894(84)90098-X.
Collatz, G.J., Berry, J.A., Clark, J.S., 1998. Effects of climate and atmospheric CO2 partial pressure on the global distribution of C4 grasses: present, past, and future. Oecologia 114, 441–454. https://doi.org/10.1007/s004420050468.
Combourieu Nebout, N., Peyron, O., Dormoy, I., 2009. Rapid climatic variability in the west Mediterranean during the last 25 000 years from high resolution pollen data. Clim. Past Discuss. 5, 671–707. https://doi.org/10.5194/cpd-5-671-2009.
Dietrich, J.D., Smith, M.D., 2016. The effect of timing of growing season drought on flowering of a dominant C4grass. Oecologia 181, 391–399. https://doi.org/10.1007/s00442-016-3579-4.
Domínguez-Villar, D., Carrasco, R.M., Pedraza, J., Cheng, H., Edwards, R.L., Willenbring, J.K., 2013. Early maximum extent of paleoglaciers from Mediterranean mountains during the last glaciation. Sci. Rep. 3, 2034. https://doi.org/10.1038/srep02034.
Ehlers, J., Gibbard, P.L., Hughes, P.D., 2011. Quaternary Glaciations - Extent and Chronology: A Closer Look. Elsevier.
Essallami, L., Sicre, M.A., Kallel, N., Labeyrie, L., Siani, G., 2007. Hydrological changes in the Mediterranean Sea over the last 30,000 years. Geochem. Geophys. Geosyst. *8*, Q07002. https://doi.org/10.1029/2007GC001587.
Feser, F., Rockel, B., von Storch, H., Winterfeldt, J., Zahn, M., 2011. Regional climate models add value to global model data: a review and selected examples. Bull. Am. Meteorol. Soc. 92, 1181–1192. https://doi.org/10.1175/2011BAMS3061.1.
Fletcher, W.J., Sánchez Goñi, M.F., 2008. Orbital- and sub-orbital-scale climate impacts on vegetation of the western Mediterranean basin over the last 48,000 yr. Quat. Res. 70, 451–464. https://doi.org/10.1016/j.yqres.2008.07.002.
Fletcher, W.J., Sánchez Goñi, M.F., Allen, J.R.M., Cheddadi, R., Combourieu-Nebout, N., Huntley, B., Lawson, I., Londeix, L., Magri, D., Margari, V., Müller, U.C., Naughton, F., Novenko, E., Roucoux, K., Tzedakis, P.C., 2010. Millennial-scale variability during the last glacial in vegetation records from Europe. Quat. Sci. Rev. 29, 2839–2864. https://doi.org/10.1016/j.quascirev.2009.11.015.
Gómez-Navarro, J.J., Bothe, O., Wagner, S., Zorita, E., Werner, J.P., Luterbacher, J., Raible, C.C., Montávez, J.P., 2015. A regional climate palaeosimulation for Europe in the period 1500-1990 - part 2: shortcomings and strengths of models and reconstructions. Clim. Past 11, 1077–1095. https://doi.org/10.5194/cp-11-1077-2015.
González-Sampériz, P., Valero-Garcés, B.L., Moreno, A., Jalut, G., García-Ruiz, J.M., Martí-Bono, C., Delgado-Huertas, A., Navas, A., Otto, T., Dedoubat, J.J., 2006. Climate variability in the Spanish Pyrenees during the last 30,000 yr revealed by the El Portalet sequence. Quat. Res. 66, 38–52. https://doi.org/10.1016/j.yqres.2006.02.004.
Gudmundsson, L., Bremnes, J.B., Haugen, J.E., Engen-Skaugen, T., 2012. Technical note: downscaling RCM precipitation to the station scale using statistical transformations - a comparison of methods. Hydrol. Earth Syst. Sci. 16, 3383–3390. https://doi.org/10.5194/hess-16-3383-2012.
Harrison, S.P., Bartlein, P.J., Izumi, K., Li, G., Annan, J., Hargreaves, J., Braconnot, P., Kageyama, M., 2015. Evaluation of CMIP5 palaeo-simulations to improve climate projections. Nat. Clim. Chang. 5, 735–743. https://doi.org/10.1038/nclimate2649.
Heinrich, H., 1988. Origin and consequences of cyclic ice rafting in the Northeast Atlantic Ocean during the past 130,000 years. Quat. Res. 29, 142–152. https://doi.org/10.1016/0033-5894(88)90057-9.
Herrera, S., Gutiérrez, J.M., Ancell, R., Pons, M.R., Frías, M.D., Fernández, J., 2012. Development and analysis of a 50-year high-resolution daily gridded precipitation dataset over Spain (Spain02). Int. J. Climatol. 32, 74–85. https://doi.org/10.1002/joc.2256.
Jalut, G., Turu I Michels, V., Dedoubat, J.J., Otto, T., Ezquerra, J., Fontugne, M., Belet, J.M., Bonnet, L., de Celis, A.G., Redondo-Vega, J.M., Vidal-Romaní, J.R., Santos, L., 2010. Palaeoenvironmental studies in NW Iberia (Cantabrian range): vegetation history and synthetic approach of the last deglaciation phases in the western Mediterranean. Palaeogeogr. Palaeoclimatol. Palaeoecol. 297, 330–350. https://doi.org/10.1016/j.palaeo.2010.08.012.
Kageyama, M., Valdes, P.J., Ramstein, G., Hewitt, C., Wyputta, U., 1999. Northern hemisphere storm tracks in present day and last glacial maximum climate simulations: a comparison of the European PMIP models. J. Clim. 12, 742–760. https://doi.org/10.1175/1520-0442(1999)012<0742:NHSTIP>2.0.CO;2.
Kageyama, M., Nebout, N.C., Sepulchre, P., Peyron, O., Krinner, G., Ramstein, G., Cazet, J.-P., 2005. The last glacial maximum and Heinrich event 1 in terms of climate and vegetation around the Alboran Sea: a preliminary model-data comparison. Comptes Rendus Geosci. 337, 983–992. https://doi.org/10.1016/j.crte.2005.04.012.
Kageyama, M., Laîné, A., Abe-Ouchi, A., Braconnot, P., Cortijo, E., Crucifix, M., de Vernal, A., Guiot, J., Hewitt, C.D., Kitoh, A., Kucera, M., Marti, O., Ohgaito, R., Otto-Bliesner, B., Peltier, W.R., Rosell-Melé, A., Vettoretti, G., Weber, S.L., Yu, Y., 2006. Last glacial maximum temperatures over the North Atlantic, Europe and western Siberia: a comparison between PMIP models, MARGO sea-surface temperatures and pollen-based reconstructions. Quat. Sci. Rev. 25, 2082–2102. https://doi.org/10.1016/j.quascirev.2006.02.010.
Ludwig, P., Schaffernicht, E.J., Shao, Y., Pinto, J.G., 2016. Regional atmospheric circulation over Europe during the last glacial maximum and its links to precipitation. J. Geophys. Res. Atmos. 121. https://doi.org/10.1002/2015JD024444.
Ludwig, P., Pinto, J.G., Raible, C.C., Shao, Y., 2017. Impacts of surface boundary conditions on regional climate model simulations of European climate during the last glacial maximum. Geophys. Res. Lett. 44, 5086–5095. https://doi.org/10.1002/2017GL073622.
Ludwig, P., Gomez-Navarro, J.J., Pinto, J.G., Raible, C.C., Wagner, S., Zorita, E., 2018. Perspectives of regional paleoclimate modelling. Ann. N. Y. Acad. Sci. https://doi.org/10.1111/nyas.13865.
Maier, A., Lehmkuhl, F., Ludwig, P., Melles, M., Schmidt, I., Shao, Y., Zeeden, C., Zimmermann, A., 2016. Demographic estimates of hunter-gatherers during the last glacial maximum in Europe against the background of palaeoenvironmental data. Quat. Int. https://doi.org/10.1016/j.quaint.2016.04.009.
Martrat, B., Jimenez-Amat, P., Zahn, R., Grimalt, J.O., 2014. Similarities and dissimilarities between the last two deglaciations and interglaciations in the North Atlantic region. Quat. Sci. Rev. 99, 122–134. https://doi.org/10.1016/j.quascirev.2014.06.016.
McManus, J.F., Francois, R., Gherardi, J.-M., Keigwin, L.D., Brown-Leger, S., 2004. Collapse and rapid resumption of Atlantic meridional circulation linked to deglacial climate changes. Nature 428, 834–837. https://doi.org/10.1038/nature02494.
Mix, A.C., Bard, E., Schneider, R., 2001. Environmental processes of the ice age: land, oceans, glaciers (EPILOG). Quat. Sci. Rev. 20, 627–657. https://doi.org/10.1016/S0277-3791(00)00145-1.
Morellón, M., Valero-Garcés, B., Vegas-Vilarrúbia, T., González-Sampériz, P., Romero, Ó., Delgado-Huertas, A., Mata, P., Moreno, A., Rico, M., Corella, J.P., 2009. Lateglacial and Holocene palaeohydrology in the western Mediterranean region: the Lake Estanya record (NE Spain). Quat. Sci. Rev. 28, 2582–2599. https://doi.org/10.1016/j.quascirev.2009.05.014.
Moreno, A., Stoll, H., Jiménez-Sánchez, M., Cacho, I., Valero-Garcés, B., Ito, E., Edwards, R.L., 2010. A speleothem record of glacial (25-11.6 kyr BP) rapid climatic changes from northern Iberian Peninsula. *Glob. Planet.* Change 71, 218–231. https://doi.org/10.1016/j.gloplacha.2009.10.002.
Moreno, A., González-Sampériz, P., Morellón, M., Valero-Garcés, B.L., Fletcher, W.J., 2012. Northern Iberian abrupt climate change dynamics during the last glacial cycle: a view from lacustrine sediments. Quat. Sci. Rev. 36, 139–153. https://doi.org/10.1016/j.quascirev.2010.06.031.
Moreno, A., Svensson, A., Brooks, S.J., Connor, S., Engels, S., Fletcher, W., Genty, D., Heiri, O., Labuhn, I., Perşoiu, A., Peyron, O., Sadori, L., Valero-Garcés, B., Wulf, S., Zanchetta, G., Allen, J.R.M., Ampel, L., Blamart, D., Birks, H., Blockley, S., ... Wohlfarth, B., 2014. A compilation of western European terrestrial records 60-8kaBP: towards an understanding of latitudinal climatic gradients. Quat. Sci. Rev. 106, 167–185. https://doi.org/10.1016/j.quascirev.2014.06.030.
Naughton, F., Sanchez Goñi, M.F., Rodrigues, T., Salgueiro, E., Costas, S., Desprat, S., Duprat, J., Michel, E., Rossignol, L., Zaragosi, S., Voelker, A.H.L., Abrantes, F., 2016. Climate variability across the last deglaciation in NW Iberia and its margin. Quat. Int. 414, 9–22. https://doi.org/10.1016/j.quaint.2015.08.073.
Ortiz, J.E., Torres, T., Delgado, A., Llamas, J.F., Soler, V., Valle, M., Julià, R., Moreno, L., Díaz-Bautista, A., 2010. Palaeoenvironmental changes in the Padul Basin (Granada, Spain) over the last 1Ma based on the biomarker content. Palaeogeogr. Palaeoclimatol. Palaeoecol. 298, 286–299. https://doi.org/10.1016/j.palaeo.2010.10.003.
Pons, A., Reille, M., 1988. The holocene- and upper pleistocene pollen record from Padul (Granada, Spain): a new study. Palaeogeogr. Palaeoclimatol. Palaeoecol. 66, 243–263. https://doi.org/10.1016/0031-0182(88)90202-7.
Prentice, I.C., Guiot, J., Harrison, S.P., 1992. Mediterranean vegetation, lake levels and palaeoclimate at the last glacial maximum. Nature 360, 658–660. https://doi.org/10.1038/360658a0.
R Core Team, 2017. A language and environment for statistical computing. R Foundation

for Statistical Computing, Vienna, Austria. https://www.R-project.org/.
Renssen, H., Isarin, R.F.B., Jacob, D., Podzun, R., Vandenberghe, J., 2001. Simulation of the younger Dryas climate in Europe using a regional climate model nested in an AGCM: preliminary results. Glob. Planet. Change 30, 41–57. https://doi.org/10.1016/S0921-8181(01)00076-5.
Rivas-Martínez, S., Rivas Sáenz, S., Penas, A., 2011. Worldwide bioclimatic classification system. Glob. Geobot. 1, 1–634. https://doi.org/10.5616/gg110001.
Rodrigo-Gámiz, M., Martínez-Ruiz, F., Rampen, S.W., Schouten, S., Sinninghe Damsté, J.S., 2014. Sea surface temperature variations in the western Mediterranean Sea over the last 20 kyr: a dual-organic proxy (UK'37 and LDI) approach. Paleoceanography 29, 87–98. https://doi.org/10.1002/2013PA002466.
Roucoux, K.H., De Abreu, L., Shackleton, N.J., Tzedakis, P.C., 2005. The response of NW Iberian vegetation to North Atlantic climate oscillations during the last 65 kyr. Quat. Sci. Rev. 24, 1637–1653. https://doi.org/10.1016/j.quascirev.2004.08.022.
Sanchez Goñi, M.F., Harrison, S.P., 2010. Millennial-scale climate variability and vegetation changes during the last glacial: concepts and terminology. Quat. Sci. Rev. 29, 2823–2827. https://doi.org/10.1016/j.quascirev.2009.11.014.
Schmidt, I., Bradtmöller, M., Kehl, M., Pastoors, A., Tafelmaier, Y., Weninger, B., Weniger, G.C., 2012. Rapid climate change and variability of settlement patterns in Iberia during the late Pleistocene. Quat. Int. 274, 179–204. https://doi.org/10.1016/j.quaint.2012.01.018.
Sepulchre, P., Ramstein, G., Kageyama, M., Vanhaeren, M., Krinner, G., Sánchez-Goñi, M.F., D'Errico, F., 2007. H4 abrupt event and late Neanderthal presence in Iberia. Earth Planet. Sci. Lett. 258, 283–292. https://doi.org/10.1016/j.epsl.2007.03.041.
Shao, Y., Anhäuser, A., Ludwig, P., Schlüter, P., Williams, E., 2018. Statistical reconstruction of global vegetation for the last glacial maximum. Glob. Planet. Chang. 168, 67–77. https://doi.org/10.1016/j.gloplacha.2018.06.002.
Sing, T., Sander, O., Beerenwinkel, N., Lengauer, T., 2005. ROCR: visualizing classifier performance in R. Bioinformatics 21, 3940–3941. https://doi.org/10.1093/bioinformatics/bti623.
Skamarock, W., Klemp, J., Dudhia, J., Gill, D., Barker, D., Wang, W., Huang, X.-Y., Duda, M., Powers, G., 2008. A Description of the Advanced Research WRF Version 3. *NCAR Tech. Note NCAR/TN-475 + STR*. 113 pp. https://doi.org/10.5065/d68s4mvh.
Stanford, J.D., Rohling, E.J., Bacon, S., Roberts, A.P., Grousset, F.E., Bolshaw, M., 2011. A new concept for the paleoceanographic evolution of Heinrich event 1 in the North Atlantic. Quat. Sci. Rev. 30, 1047–1066. https://doi.org/10.1016/j.quascirev.2011.02.003.
Stevens, B., Giorgetta, M., Esch, M., Mauritsen, T., Crueger, T., Rast, S., Salzmann, M., Schmidt, H., Bader, J., Block, K., Brokopf, R., Fast, I., Kinne, S., Kornblueh, L., Lohmann, U., Pincus, R., Reichler, T., Roeckner, E., 2013. Atmospheric component of the MPI-M earth system model: ECHAM6. J. Adv. Model. Earth Syst. 5, 146–172. https://doi.org/10.1002/jame.20015.
Strandberg, G., Brandefelt, J., Kjellström, E., Smith, B., 2011. High-resolution regional simulation of last glacial maximum climate in Europe. *Tellus Ser. A Dyn.* Meteorol. Oceanogr. 63, 107–125. https://doi.org/10.1111/j.1600-0870.2010.00485.x.
Tallavaara, M., Luoto, M., Korhonen, N., Järvinen, H., Seppä, H., 2015. Human population dynamics in Europe over the last glacial maximum. Proc. Natl. Acad. Sci. 112, 8232–8237. https://doi.org/10.1073/pnas.1503784112.
Teutschbein, C., Seibert, J., 2012. Bias correction of regional climate model simulations for hydrological climate-change impact studies: review and evaluation of different methods. J. Hydrol. 456–457, 12–29. https://doi.org/10.1016/j.jhydrol.2012.05.052.
Turrero, P., Dominguez-Cuesta, M.J., Jimenez-Sanchez, M., Garcia-Vazquez, E., 2013. The spatial distribution of Palaeolithic human settlements and its influence on palaeoecological studies: a case from northern Iberia. J. Archaeol. Sci. 40, 4127–4138. https://doi.org/10.1016/j.jas.2013.06.003.
UNEP, 1992. *World Atlas of Desertification*. Edward Arnold. Retrieved from. https://catalogue.nla.gov.au/Record/624121.
Valero-Garcés, B.L., González-Sampériz, P., Navas, A., Machin, J., Delgado-Huertas, A., Pena-Monné, J.L., Sancho-Marcén, C., Stevenson, T., Davis, B., 2004. Paleohydrological fluctuations and steppe vegetation during the last glacial maximum in the Central Ebro valley (NE Spain). Quat. Int. 122, 43–55. https://doi.org/10.1016/j.quaint.2004.01.030.
Vegas, J., Ruiz-Zapata, B., Ortiz, J.E., Galán, L., Torres, T., García-Cortés, Á., Gil-García, M.J., Pérez-González, A., Gallardo-Millán, J.L., 2010. Identification of arid phases during the last 50-cal. ka BP from the Fuentillejo maar-lacustrine record (Campo de Calatrava Volcanic Field, Spain). J. Quat. Sci. 25, 1051–1062. https://doi.org/10.1002/jqs.1262.